

# Probing time delay of strong-field resonant above-threshold ionization\*

Shengliang Xu(徐胜亮)<sup>1</sup>, Qingbin Zhang(张庆斌)<sup>1,†</sup>, Cheng Ran(冉成)<sup>1</sup>,  
Xiang Huang(黄湘)<sup>1</sup>, Wei Cao(曹伟)<sup>1</sup>, and Peixiang Lu(陆培祥)<sup>1,2</sup>

<sup>1</sup>School of Physics and Wuhan National Laboratory for Optoelectronics, Huazhong University of Science and Technology, Wuhan 430074, China

<sup>2</sup>Hubei Key Laboratory of Optical Information and Pattern Recognition, Wuhan Institute of Technology, Wuhan 430205, China

(Received 27 September 2020; revised manuscript received 30 October 2020; accepted manuscript online 5 November 2020)

The high-resolution three-dimensional photoelectron momentum distributions via above-threshold ionization (ATI) of Xe atoms are measured in an intense near circularly polarized laser field using velocity map imaging and tomography reconstruction. Compared to the linearly polarized laser field, the employed near circularly polarized laser field imposes a more strict selection rule for the transition via resonant excitation, and therefore we can selectively enhance the resonant ATI through certain atomic Rydberg states. Our results show the self-reference ionization delay, which is determined from the difference between the measured streaking angles for nonadiabatic ATI via the 4f and 5f Rydberg states, is 45.6 as. Our method provides an accessible route to highlight the role of resonant transition between selected states, which will pave the way for fully understanding the ionization dynamics toward manipulating electron motion as well as reaction in an ultrafast time scale.

**Keywords:** above threshold ionization, resonant ionization delay, transition selection rule

**PACS:** 32.80.-t, 32.80.Ee, 32.80.Rm

**DOI:** 10.1088/1674-1056/abc7a5

## 1. Introduction

Ionization stands out as one of the most fundamental processes in light-matter interaction,<sup>[1,2]</sup> since it triggers the subsequent electron dynamic in the continuum, and therefore affects many important processes such as photoelectron holography,<sup>[3,4]</sup> high-harmonic generation,<sup>[5,6]</sup> and non-sequential double ionization.<sup>[7–10]</sup> For this reason, resolving the ionization process in its inherent ultrafast time scale becomes key for understanding and steering free-electron dynamics as well as reactions. The advanced attosecond metrologies, for example, reconstruction of attosecond beating by interference of two-photon transitions (RABBITT) and attosecond streaking (AS), have made it possible to measure the ionization process in attosecond resolution. With these technologies, a noticeable delay in photoemission from the ground state to continuum for atoms, molecules, and solids was observed.<sup>[11–15]</sup>

As compared to releasing the photoelectron directly into the continuum, the electron may also be first promoted to laser dressed intermediate state via resonant excitation, and then released into the continuous state in the laser field.<sup>[16]</sup> The involution of intermediate states introduces an additional phase during the transition, which is believed to relate to the predicted extra delay.<sup>[9,17,18]</sup> In fact, the experimentally measured ionization delay contains contributions from both the intrinsic ionization delay and the extracted time

delay induced by the coupling of the long-range Coulomb and the laser field.<sup>[20,21]</sup> The former one is also known as quantum-mechanical Eisenbud–Wigner–Smith (EWS) delay, which provides unique insight into the structural and transport dynamics in systems.<sup>[22–24]</sup> The latter one is assumed physically unimportant but cannot be excluded in the presence of a strong laser field. To disentangle the two contributions and resolve the intrinsic ionization dynamics, experimentally, the noble gas atoms have been adopted as a benchmark to calibrate the measured delays in more complicated systems.<sup>[25]</sup> Alternatively, a self-referenced measurement is implemented for different resonant channels, and thereby highlighting the relative ionization time delay between different pathways. A recent experiment observed the Freeman resonance delay between ionization through 4f and 5p Rydberg states of argon is  $140 \pm 40$  as.<sup>[19]</sup>

So far, most studies related to the measurement of Freeman resonant ionization dynamics rely on attosecond pump-probe method with linearly polarized light.<sup>[19,26]</sup> While the angular streaking method is a relatively simple method, which provides the attosecond time resolution without the explicit need of attosecond pulses.<sup>[27,28]</sup> This approach defines a good mapping relationship between instant of ionization and final angle of the momentum vector in a near circularly polarized laser field, offering a time resolution of a few attoseconds.<sup>[29]</sup> Using this method, considerable research efforts have been

\*Project supported by the National Natural Science Foundation of China (Grant Nos. 11574101, 11674116, 11774111 and 11934006), the Open Fund of Hubei Provincial Key Laboratory of Optical Information and Pattern Recognition (Grant No. 201902), and the International Cooperation Program of Hubei Innovation Fund (Grant No. 2019AHB052).

†Corresponding author. E-mail: zhangqingbin@hust.edu.cn

devoted to time measurement of the release of electron directly from the ground state to the continuous state or verify the nonadiabaticity in a strong field, with Keldysh parameters spans from 0.1 up to 4.<sup>[30]</sup> In this paper, by employing a near circularly polarized laser field, angular resolved photoelectron momentum distribution (PMD) is measured, allowing us to look into the ultrafast ionization dynamics. More importantly, the use of the near circularly polarized laser field provides us a unique opportunity to select the specific intermediate states, for example, 4f and 5f Rydberg states in our work. Thus it will facilitate refining experimental observations and deepen the understanding of the role of resonant transition during ATI.

## 2. Experimental setup

The laser pulses used for the implementation of the experiment are generated from a Ti:sapphire laser system, and then they are frequency doubled to 410 nm ( $\hbar\omega = 3.03$  eV) with a 300  $\mu\text{m}$ -thick  $\beta$ -barium-borate crystal. The linearly polarized laser pulse is converted into right elliptically polarized (REP) light by passing through a  $\lambda/4$  waveplate, with the ellipticity  $\varepsilon = 0.7$ . The laser pulse used in our experiment is characterized by the home-made cross-correlation frequency-resolved optical gating (XFROG) technique and the pulse duration is 115 fs. The laser is focused onto the supersonic Xe gas beam by a plano-convex lens ( $f = 30$  cm) to measure the projected PMD with velocity map imaging (VMI) as shown in Fig. 1(b). To obtain the three-dimensional PMD by applying the tomographic reconstruction, the acquisition of the projected PMDs under a number of angles is required.<sup>[31–33]</sup> This multiangle measurement is achieved by rotating the polarization of laser with a  $\lambda/2$  waveplate mounted on a motorized rotation stage at a step size of  $0.1^\circ$ .

## 3. Results and discussion

The Keldysh parameter  $\gamma$  (nonadiabatic factor) is calculated to be 2.78 with our laser parameters. Here, we generalize the static picture of tunneling into the nonadiabatic regime. To make the ionization process clearer and more intuitive, the interpretation of nonadiabatic tunneling as absorption of photons followed by tunneling with 4f and 5f intermediate states is shown in Fig. 1(a). We first discuss the selection of the specific intermediate states using REP laser field. As we all know, when electron's spin is parallel to its orbital angular momentum, removing a valence electron from Xe could yield the ground state of the ion (ionization potential  $I_p = 12.13$  eV with total angular momentum  $J = 3/2$ ), while the emission of an electron with opposite spin ( $j = 1/2$ ) leads to the first excited state of the ion (total angular momentum  $J = 1/2$ ).<sup>[34]</sup> The two combs of ATI peaks belonging to two ionic states ( $J = 3/2$  and  $J = 1/2$ ) with an energy difference of 1.31 eV do not overlap in our photoelectron energy spectrum.<sup>[35]</sup> Since the measured energy difference of two ATI peaks via 4f and 5f intermediate states belonging to ionic ground state is only 0.37 eV, which is much less than 1.31 eV, we therefore only concentrate on the PMD belonging to the ionic ground state. Corresponding to the ionic ground state, there exists three degenerate  $p$  orbitals of valence electron for Xe, the  $p_+$  orbital ( $m = +1$ ),  $p_-$  orbital ( $m = -1$ ), and  $p_0$  orbital ( $m = 0$ ). The magnetic quantum number  $m = -1$  ( $m = +1$ ) refers to the projection of the angular momentum in the quantization axis ( $z$  axis, light propagation direction) is  $-1$  ( $+1$ ), which means that the electron ring currents in polarization plane ( $xy$  plane) is counter-rotating (co-rotating) in the sense as the REP field. In practice, the ionization of  $p_0$  orbital is strongly suppressed and therefore neglected.<sup>[36]</sup> To resonantly ionize Xe, four 410-nm photons are required to first promote valence electron from the ground state to intermediate state, and then the electron is liberated into continuum nonadiabatically in laser field. For linearly polarized light, this four-photon excitation is allowed between states that are the same in the parity, therefore,  $|p, \pm 1\rangle$ ,  $|f, \pm 1\rangle$ ,  $|h, \pm 1\rangle$ ,  $|f, \pm 3\rangle$ ,  $|h, \pm 3\rangle$  and  $|h, \pm 5\rangle$  states can be populated during the process of ionization. While the selection rule is more strict for circularly polarized light, that is, the absorption of one photon of circularly polarized light will change the magnetic quantum number either by  $+1$  or  $-1$  monotonously. For the REP field used in our experiment, the absorption of one photon for resonant ionization is assumed to increase the magnetic quantum number by  $\Delta m = +1$ . Therefore, the number of intermediate states plays in the role that can be cut down and the analysis would be simple. In this case, the accessible intermediate states become sensitive to the helicity of initial  $p$  orbital. The possible excitation pathways are  $|p, -1\rangle \rightarrow |f, +3\rangle$ ,  $|p, -1\rangle \rightarrow |h, +3\rangle$  and  $|p, +1\rangle \rightarrow |h, +5\rangle$ . Because of the dynamic Stark effect in the presence of strong

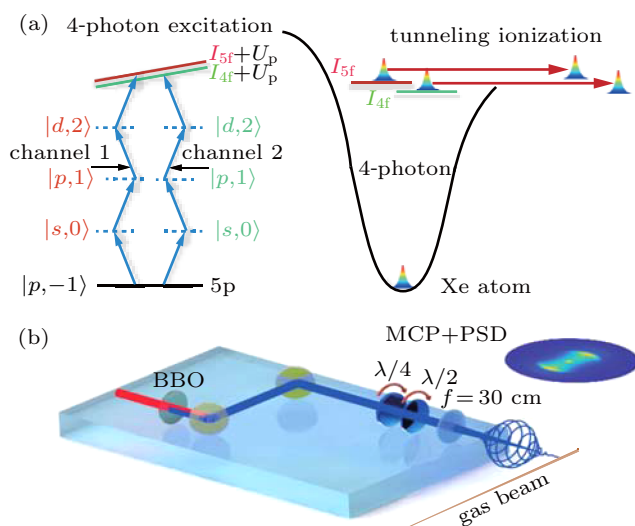


**Fig. 1.** (a) The interpretation of nonadiabatic tunneling as absorption of photons followed by tunneling with 4f and 5f intermediate states. (b) Schematic view of the experimental setup.

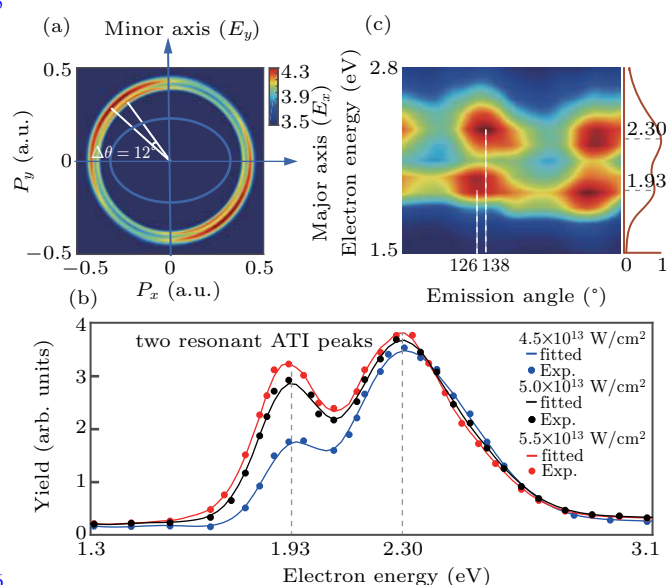
laser field, the bound intermediate states  $|h, +3\rangle$ ,  $|h, +5\rangle$  and  $|f, +3\rangle$  of Xe all shift upward along with the ionization potential by approximately  $U_p = e^2 I / (2cm\epsilon_0\omega^2)$  with the electric permittivity of free space  $\epsilon_0$ , the speed of light  $c$ , the charge  $e$ , mass  $m$  of the electron, the laser intensity  $I$  and angular frequency  $\omega$ . Compared to the  $h$  series states, the  $f$  series states with originally lower energy need to be lifted more to match the energy of the four photons. Therefore, the resonant ionization of  $f$  series states requires higher laser intensity, resulting in a much higher ionization rate at resonance due to the highly nonlinear ionization rate as a function of intensity. Among all the  $f$  series Rydberg states, achieving resonance with the lowest-lying  $4f$  and  $5f$  states requires the highest laser intensity which leads to highest yield. Meanwhile the energy difference of these two states is largest. Thus the resonant ionization pathways via  $5f$  (channel 1) and  $4f$  (channel 2) states shown in Fig. 1(a) are easiest to identify in the measured PMD.

Figure 2(a) shows the measured PMD in REP laser field at  $5.5 \times 10^{13}$  W/cm<sup>2</sup>. We can clearly see that the PMD exhibits an obvious double-ring structure, and energy separation of the double rings is approximately 0.32 eV, which matches well with the energy separation of  $4f$  and  $5f$  energy levels available in the National Institute of Standards and Technology (NIST).<sup>[37]</sup> The double-ring ATI structure in PMD originated from resonant excitation via the intermediate  $4f$  and  $5f$  states is also supported by the fact that these two ATI ring energies are independent of intensity,<sup>[38]</sup> as shown in Fig. 2(b) and Fig. 3. In earlier studies, two scenarios were suggested for explaining the intensity-independent rings in resonant ATI. First, one

assumes that electron ionizes from an excited state to a continuous state before the intensity has considerably changed. The resonance condition can be fulfilled somewhere in the laser focus when the peak intensity is higher than the resonant value. The second scenario<sup>[40]</sup> suggests that a high-lying Rydberg state can be shifted upwards almost as much as the continuum level and give rise to intensity-independent peak positions. To quantify the observed two resonant ATI rings, we further depict the angle- and energy-resolved photoelectron spectrum in Fig. 2(c). We can clearly find considerable angular offset difference for two rings with close energies. This offset angle is expected to reflect the ionization time difference between the two ionization channels, according to the mapping relationship  $\Delta\theta = \omega\Delta t$  in angular streaking. In angular streaking, the electron is born necessarily at the peak of electric field, in order to assign unambiguously the most probable photoemission offset angle to the moment when the laser field reaches its peak. To verify this, we experimentally compared the PMD of a circularly polarized laser field with that of a near-circularly polarized laser field. For every cyclic structure, there are two peaks which are almost centrosymmetric with respect to the zero momentum in the PMD in

near-circularly polarized laser field (Fig. 2(a)), while the PMD is isotropous in circularly polarized laser field (not shown). This result evidently suggests that the two-peak angular distribution is a consequence of the major axis of the polarization ellipse. It must also be mentioned that the momentum of the most probable electrons, which is determined by the vector potential of the light field along major axis of the polarization ellipse, deviates from the minor axis of the polarization ellipse. This deviation is believed to be due to the Coulomb interaction and the nonadiabatic effect during the ionization process.<sup>[30]</sup> In the application of timing absolute ionization time delay, therefore it is necessary to precisely calibrate the deviation angle with respect to the minor axis of the polarization ellipse, in order to determine time zero.<sup>[41]</sup> However, the calibration is nontrivial. Until recently, several schemes rely on two-color circularly polarized laser field, which was proposed for achieving an easier and better calibration.<sup>[42,43]</sup>

Here, we extract considerable offset angle difference between two resonant ionization channels with very close energy. Since we measure the difference, we do not need to calibrate the deflection angle for each ionization channel. They are automatically eliminated in the process of subtracting for obtaining relative ionization time, as long as the Coulomb attractions are similar for the two ionization pathways, which has been proved in the following paragraphs. When involving the excited intermediate states, the electron motions under the barrier can be much more complex. The 45.6 as time difference,



**Fig. 2.** (a) Measured PMD of the ATI belonging to the  $2P^{3/2}$  ionic state in polarization plane ( $x$ - $y$  plane) with  $|P_z| < 0.92$  a.u. The offset angle difference  $\Delta\theta$  of two ionization channels ( $4f$  and  $5f$ ) is  $12^\circ$ . The blue curve represents the elliptically polarized light field. (b) The measured photoelectron energy distributions with the laser intensities from  $4.5 \times 10^{13}$  W/cm<sup>2</sup> to  $5.5 \times 10^{13}$  W/cm<sup>2</sup>. The two resonant ATI peaks are labeled by two grey dotted lines. (c) Measured photoelectron energy distribution with the emission angle from  $5^\circ$  to  $355^\circ$ . The laser intensity is  $5.5 \times 10^{13}$  W/cm<sup>2</sup> for both (a) and (c).

228 reading out from the  $12^\circ$  offset angle difference, is strong ex-  
 229 perimental evidence of how intermediate states affect the ATI  
 230 process.

231 Next, we prove that the Coulomb interactions for two ion-  
 232 ization channels are similar. As we know that the Coulomb in-  
 233 teraction between the parent ion and electron is very sensitive  
 234 to the electron's kinetic energy. Usually, the slower (faster)  
 235 electrons will be more strongly (more weakly) deflected. In  
 236 the earlier studies, it has been demonstrated that intensity is  
 237 a useful knob to shift the position of ATI peak in the energy  
 238 domain due to the pondermotive energy shift.<sup>[44,45]</sup> Therefore,  
 239 the Coulomb effect can be compared between ATI peaks with  
 240 very close energies by changing laser intensity slightly. We  
 241 first show how the ATI peaks are shifted in the energy do-  
 242 main by varying the laser intensity from  $2.6 \times 10^{13}$  W/cm<sup>2</sup> to  
 243  $8.4 \times 10^{13}$  W/cm<sup>2</sup> in Fig. 3. The results are obtained by solv-  
 244 ing the time-dependent Schrödinger equation for Xe atom as  
 245 given by

$$246 \quad i\partial\psi(\mathbf{r},t)/\partial t = [-\nabla^2/2 + V_C(\mathbf{r}) + V_E(\mathbf{r},t)]\psi(\mathbf{r},t), \quad (1)$$

247 where  $V_C(\mathbf{r})$  represents the model potential and  $V_E(\mathbf{r},t)$  de-  
 248 scribes the dipole potential in the external laser field. To ac-  
 249 count for the correct energy of the Xe 5p orbital of  $-0.446$  a.u.  
 250 ( $-12.13$  eV), the model potential which is similar to the em-  
 251 pirical three-dimensional potential in Refs. [46,47] is em-  
 252 ployed. However, due to the lower dimensionality the soft  
 253 core parameters are modified. The effective model potential  
 254  $V_c$  of xenon is therefore given by

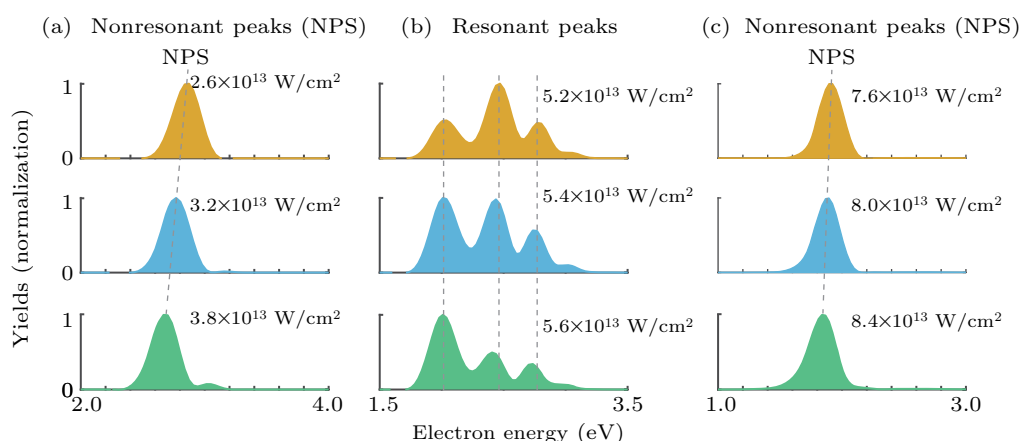
$$255 \quad V_c = -(1 + 2\exp(-(x^2 + y^2)))/\sqrt{(x^2 + y^2 + 0.2)} \quad (2)$$

256 with the soft-core parameter of 0.2. The Xe atom is exposed  
 257 to the REP laser field with

$$258 \quad \mathbf{E}(t) = \frac{1}{\sqrt{1 + \varepsilon^2}} E_0 \sin^2\left(\frac{t\pi}{\tau}\right) \cos(\omega t) \mathbf{e}_x$$

$$+ \frac{\varepsilon}{\sqrt{1 + \varepsilon^2}} E_0 \sin^2\left(\frac{t\pi}{\tau}\right) \sin(\omega t) \mathbf{e}_y. \quad (3)$$

260 Here,  $E_0$  is the amplitude, the ellipticity  $\varepsilon$  is 0.7,  $\omega$  is the  
 261 angular frequency,  $\tau$  is the total duration of the laser pulse  
 262 (here,  $T = 2\pi/\omega$ ). We utilize the split-step Fourier method  
 263 to numerically solve Eq. (2) integrated in a two-dimensional  
 264 grid using the single-active-electron (SAE) approximation.<sup>[48]</sup>  
 265 The numerical grid is integrated from  $-L_0/2$  ( $-204.7$  a.u.)  
 266 to  $L_0/2$  ( $204.7$  a.u.), with a grid spacing of 0.2 a.u. for  
 267 each dimension and a time step of 0.04 a.u. The basis set  
 268 of  $p_x$  and  $p_y$  is obtained by an imaginary time propagation  
 269 method.<sup>[49]</sup> In order to compare with the experimental exci-  
 270 tation process ( $|p, -1\rangle \rightarrow |f, +3\rangle$ ), we only pay attention to  
 271 the initial orbital with magnetic quantum number  $m = -1$  in  
 272 our model. The initial orbital prepared for solving the TDSE  
 273 is  $p(m = -1) = (p_x - ip_y)/\sqrt{2}$ . In Figs. 3(a) and 3(c), due  
 274 to pondermotive energy shift, the ATI peak moves towards  
 275 lower energy with the increase of laser intensity. However,  
 276 the positions of the main three peaks are independent of laser  
 277 intensity as shown in Fig. 3(b), which indicates that the res-  
 278 onant ionization occurs with these laser intensities. In these  
 279 two-dimensional numerical calculations, we find the ATI peak  
 280 splits into three sub-peaks, which coincide with the resonant  
 281 excitation with the three intermediate states of magnetic quan-  
 282 tum number  $m = 3$ . The energies of these three intermediate  
 283 states are  $-1.10$ ,  $-0.69$  and  $-0.42$  eV, respectively. In the ex-  
 284 periment, the energies of 4f, 5f and 6f are  $-0.86$ ,  $-0.55$  and  
 285  $-0.39$  eV, respectively. The 6f resonant peak is close to the 5f  
 286 resonant peak. Therefore, it can not be resolved in the mea-  
 287 sured photoelectron energy spectrum when it is much lower  
 288 than the 5f resonant peak. The energies of the states of model  
 289 Xe are obtained by diagonalizing the Hamiltonian containing  
 290 model potential  $V_c$  as summarized in Table 1. The positions  
 291 of three resonant peaks are labeled by the gray dashed lines  
 292 in Fig. 3(b). It is also noticed that the second and third peaks



294

295 **Fig. 3.** (a)–(c) The simulated photoelectron energy distributions with the laser intensities from  $2.6 \times 10^{13}$  W/cm<sup>2</sup> to  $8.4 \times 10^{13}$  W/cm<sup>2</sup>. The yield is normalized for each laser intensity.

of each resonant ATI deviate slightly from the predicted dashed lines at the laser intensities of  $5.4 \times 10^{13}$  W/cm<sup>2</sup> and  $5.6 \times 10^{13}$  W/cm<sup>2</sup>, this is because each peak is also influenced by the falling edge of the peak in front. Using whether the ATI peak position shifts with the variation of laser intensity as the criterion, we can clearly identify the ranges of laser intensity which are responsible for the resonant and nonresonant ionization.

**Table 1.** Energies (eV) of the first 6 lowest-lying eigenstates for  $m = 0, \pm 1, \pm 2, \pm 3, \pm 4$ .

Number	$m = 0$	$m = \pm 1$	$m = \pm 2$	$m = \pm 3$	$m = \pm 4$
1	-53.90	-12.13	-2.18	-1.10	-0.67
2	-5.51	-2.94	-1.12	-0.69	-0.44
3	-2.06	-1.36	-0.67	-0.42	-0.21
4	-1.07	-0.78	-0.42	-0.16	0.11
5	-0.65	-0.49	-0.13	0.19	0.51
6	-0.38	-0.21	0.26	0.64	0.99

We then compare the influence of the Coulomb deflection for the resonant ionization with different laser intensities. When laser intensity changes from  $4.5 \times 10^{13}$  W/cm<sup>2</sup> to  $5.5 \times 10^{13}$  W/cm<sup>2</sup>, the offset angle difference  $\Delta\theta$  of two ionization channels is  $12^\circ$  for three laser intensities.

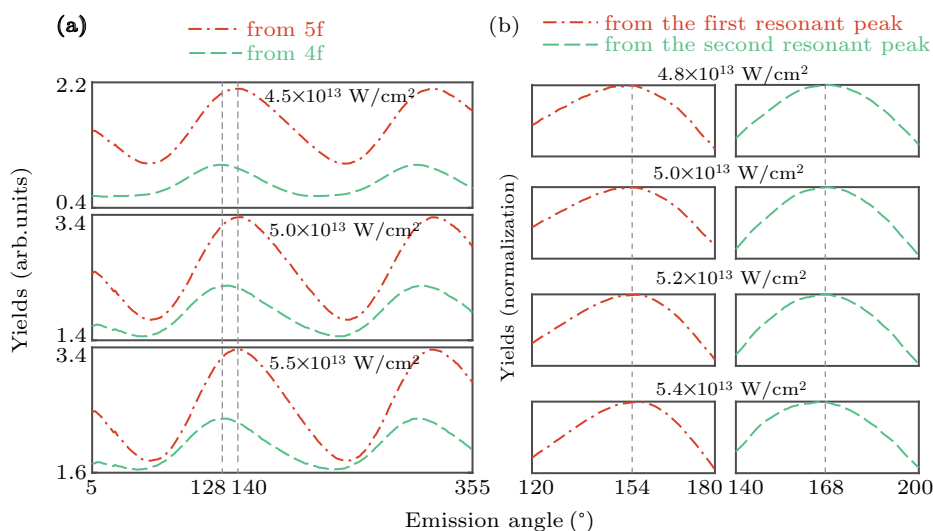
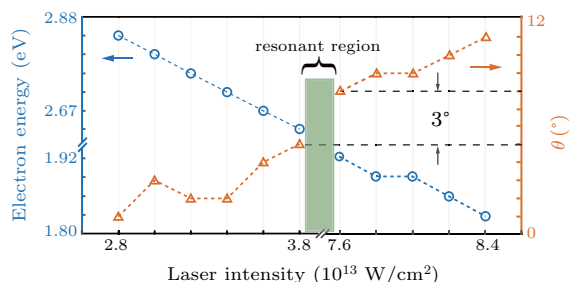


**Fig. 4.** (a) The measured photoelectron angular distributions with the laser intensities of  $4.5 \times 10^{13}$  W/cm<sup>2</sup>,  $5.0 \times 10^{13}$  W/cm<sup>2</sup> and  $5.5 \times 10^{13}$  W/cm<sup>2</sup>. The offset angle difference  $\Delta\theta$  of two ionization channels is  $12^\circ$  for three laser intensities. The photoelectron angular distributions via 4f and 5f intermediate states are labeled by the green dashed line and red dot-dashed line. (b) The simulated photoelectron angular distributions with the laser intensities of  $4.8 \times 10^{13}$  W/cm<sup>2</sup>,  $5.0 \times 10^{13}$  W/cm<sup>2</sup>,  $5.2 \times 10^{13}$  W/cm<sup>2</sup> and  $5.4 \times 10^{13}$  W/cm<sup>2</sup>. The offset angle difference  $\Delta\theta$  of the two ionization channels is  $14^\circ$  for four laser intensities.

We finally turn to estimate how much offset angle difference will be introduced by the Coulomb deflection for the two resonant ionization channels mentioned above. For these two resonant ionization channels, the offset angle difference is contributed by both resonant ionization delay and different Coulomb deflections. If the difference on Coulomb deflection is small enough, then the difference on the offset angle can be attributed to the ionization time delay for the two resonant channels. To extract the Coulomb deflection difference, we compare the offset angle between two nonresonant ATI peaks, the energy of which is lower and higher than the resonant ATI peaks. In principle, the Coulomb deflection induced difference on the offset angle should be larger for these two selected

356 ergy difference will not exceed this value. Recalling the fact  
 357 that the offset angle difference between the resonant 4f and 5f  
 358 ATI peaks is greater than  $10^\circ$  both in experiment and numer-  
 359 ical simulation, we can conclude that this offset angle differ-  
 360 ence is mainly contributed by the ionization delay between the  
 361 two resonant ionization channels.



362 **Fig. 5.** The simulated final energy and offset angle of the ATI peak for  
 363 initial  $|p, m = -1\rangle$  state electrons are shown in this part. The laser intensi-  
 364 ties are from  $2.8 \times 10^{13}$  W/cm<sup>2</sup> to  $8.4 \times 10^{13}$  W/cm<sup>2</sup>. The predicted  
 365 position of resonant region is labeled by a green rectangle. The minimum  
 366 value of the longitudinal axis for the offset angle is set to 0. The  
 367 offset angle difference for the two boundaries of the resonant region is  
 368 labeled by black dashed lines.

#### 364 4. Conclusion

365 In summary, we have experimentally observed a 45.6 as  
 366 difference of strong-field ionization time via the field-dressed  
 367 4f and 5f states of Xe atoms. The REP field allows us to un-  
 368 ambiguously select specific resonant intermediate states in the  
 369 self-reference measurement. The selected states differ only  
 370 in principal quantum number while have the same magnetic  
 371 quantum number, which is in favor of highlighting the role  
 372 of the radial part of electron orbital during resonant excita-  
 373 tion. Our findings advance the understanding of sub-cycle  
 374 photoionization dynamics, and shed light on the manipulation  
 375 of ultrafast electron dynamics in laser-matter interactions.

#### References

- [1] Vasa P and Lienau C 2017 *ACS Photon.* **5** 2
- [2] Kinyua D M, Niu L, Long H, Wang K and Wang B 2019 *Opt. Mater.* **96** 109311
- [3] Barton J J 1988 *Phys. Rev. Lett.* **61** 1356
- [4] He M, Li Y, Zhou Y, Li M, Cao W and Lu P 2018 *Phys. Rev. Lett.* **120** 133204
- [5] Paul P M, Toma E S, Breger P, Mullot G, Augé F, Balcou Ph, Muller H G and Agostini P 2001 *Science* **292** 1689
- [6] Li J, Zhang Q, Li L, Zhu X, Huang T, Lan P and Lu P 2019 *Phys. Rev. A* **99** 033421
- [7] Walker B, Sheehy B, DiMauro L F, Agostini P, Schafer K J and Kulan-der K C 1994 *Phys. Rev. Lett.* **73** 1227
- [8] Eckart S, Richter M, Kunitski M, Hartung A, Rist J, Henrichs K, Schlott N, Kang H, Bauer T, Sann H, Schmidt L Ph H, Schöffler M, Jahnke T and Dörner R 2016 *Phys. Rev. Lett.* **117** 133202
- [9] Huang X, Zhang Q, Xu S, Fu X, Han X, Cao W and Lu P 2019 *Opt. Express* **27** 38116
- [10] Feng Y, Li M, Luo S, Liu K, Du B, Zhou Y and Lu P 2019 *Phys. Rev. A* **100** 063411
- [11] Cavalieri A L, Muller N, Uphues T, Yakovlev V S, Baltuska A, Horvath B, Schmidt B, Blumel L, Holzwarth R, Hendel S, Drescher M, Kleineberg U, Echenique P M, Kienberger R, Krausz F and Heinzmann U 2007 *Nature* **449** 1029
- [12] Schultze M, Fiess M, Karpowicz N, Gagnon J, Korbman M, Hofstetter M, Neppl S, Cavalieri A L, Komminos Y, Mercouris T, Nicolaides C A, Pazourek R, Nagele S, Feist J, Burgdorfer J, Azzeer A M, Ernstorfer R, Kienberger R, Kleineberg U, Goulielmakis E, Krausz F and Yakovlev V S 2010 *Science* **328** 1658
- [13] Klunder K, Dahlstrom J M, Gisselbrecht M, Fordell T, Swboda M, Guenot D, Johnsson P, Caillat J, Mauritsson J, Maquet A, Taieb R and L'Huillier A 2011 *Phys. Rev. Lett.* **106** 143002
- [14] Locher R, Castiglioni L, Lucchini M, Greif M, Gallmann L, Osterwalder J, Hengsberger M and Keller U 2015 *Optica* **2** 405
- [15] Kasmi L, Lucchini M, Castiglioni L, Kliuiev P, Osterwalder J, Hengsberger M, Gallmann L, Krüger P and Keller U 2017 *Optica* **4** 1492
- [16] Freeman R R, Bauksbaum P H, Milchberg H, Darack S, Schumacher D and Geusic M E 1987 *Phys. Rev. Lett.* **59** 1092
- [17] Zao T, Chen C, Szilvasi T, Keller M, Mavrikakis M, Kapteyn H and Murnane M 2016 *Science* **353** 62
- [18] Huppert M, Jordan I, Baykuseva D, von Conta A and Worner H J 2016 *Phys. Rev. Lett.* **117** 093001
- [19] Gong X C, Lin C, He F, Song Q Y, Lin K, Ji Q Y, Zhang W B, Ma J Y, Lu P F, Liu Y Q, Zeng H P, Yang W F and Wu J 2017 *Phys. Rev. Lett.* **118** 143203
- [20] Feist J, Zatsarinny O, Nagele S, Pazourek R, Burgdorfer J, Guan X X, Bartschat K and Schneider B I 2014 *Phys. Rev. A* **89** 033417
- [21] Song X H, Shi G L, Zhang G J, Xu J W, Lin C, Chen J and Yang W F 2018 *Phys. Rev. Lett.* **121** 103201
- [22] Eisenbud L 1948 *Formal properties of nuclear collisions* (Ph.D. Dissertation) (Princeton, NJ: Princeton University, Princeton, NJ)
- [23] Wigner E P 1955 *Phys. Rev.* **98** 145
- [24] Smith F T 1960 *Phys. Rev.* **118** 349
- [25] Seiffert L, Liu Q, Zherebtsov S, Trabattini A, Rupp P, Castrovillani M C, Galli M, Süßmann F, Wintersperger K, Stierle J, Sansone G, Poletto L, Frassetto F, Halfpap I, Mondes V, Graf C, Rühl E, Krausz F, Nisoli M, Fennel T, Calegari F and Kling M F 2017 *Nat. Phys.* **13** 766
- [26] Ge P P, Han M, Liu M M, Gong Q H and Liu Y Q 2018 *Phys. Rev. A* **98** 013409
- [27] Eckle P, Pfeiffer A N, Cirelli C, Staudte A, Dörner R, Müller H G, Buttiker M and Keller U 2008 *Science* **322** 1525
- [28] Pfeiffer A N, Cirelli C, Smolarski M, Dimitrovski D, Abu-Samaha M, Madsen L B and Keller U 2012 *Nat. Phys.* **8** 76
- [29] Pfeiffer A N, Cirelli C, Smolarski M and Keller U 2013 *Chem. Phys.* **414** 84
- [30] Klaiber M, Hatsagortsyan K Z and Keitel C H 2015 *Phys. Rev. Lett.* **114** 083001
- [31] Eppink A and Parker D H 1997 *Rev. Sci. Instrum.* **68** 3477
- [32] Smeenk C, Arissian L, Staudte A, Villeneuve D and Corkum P 2009 *J. Phys. B* **42** 185402
- [33] Wollenhaupt M, Krug M, Köhler J, Bayer T, Sarpe-Tudoran C and Baumert T 2009 *Appl. Phys. B* **95** 647
- [34] Bordas C, Paulig F, Helm H and Huestis D L 1996 *Rev. Sci. Instrum.* **67** 2257
- [35] Trabert D, Hartung A, Eckart S, Trinter F, Kalinin A, Schöffler M, Schmidt L Ph H, Jahnke T, Kunitski M, and Dörner R 2018 *Phys. Rev. Lett.* **120** 043202
- [36] Barth I and Smirnova O 2011 *Phys. Rev. A* **84** 063415
- [37] Available at [http://physics.nist.gov]
- [38] Rudenko A, Zrost K, Schröter C D, de Jesus V L B, Feuerstein B, Moshhammer R and Ullrich J 2004 *J. Phys. B* **37** L407
- [39] Gibson G N, Freeman R R and McItrath T J 1992 *Phys. Rev. Lett.* **69** 1904
- [40] de Boer M P and Müller H G 1992 *Phys. Rev. Lett.* **68** 2747
- [41] Boge R, Cirelli C, Landsman A S, Heuser S, Ludwig A, Maurer J, Weger M, Gallmann L and Keller U 2013 *Phys. Rev. Lett.* **111** 103003
- [42] Eicke N and Lein M 2019 *Phys. Rev. A* **99** 031402
- [43] Ge P, Han M, Deng Y, Gong Q and Liu Y 2019 *Phys. Rev. Lett.* **122** 013201
- [44] Krajewska K, Fabrikant I I and Starace A F 2012 *Phys. Rev. A* **86** 053410
- [45] Hüter O and Temps, F 2017 *Rev. Sci. Instrum.* **88** 046101
- [46] Tong X and Lin C 2005 *J. Phys. B* **38** 2593
- [47] Zhang Q, Lan P and Lu P 2014 *Phys. Rev. A* **90** 043410
- [48] Feit M, Fleck Jr J and Steiger A 1982 *J. Comput. Phys.* **47** 412
- [49] Protopapas M, Keitel C H and Knight P L 1997 *Rep. Prog. Phys.* **60** 389